

NOTES AND CORRESPONDENCE

Exploration of the MODIS Cloud-Top Property Products for the Investigation of Equatorial Wave Systems

YUE LI, GERALD R. NORTH, AND PING YANG

Department of Atmospheric Sciences, Texas A&M University, College Station, Texas

BRYAN A. BAUM

Space Science and Engineering Center, University of Wisconsin—Madison, Madison, Wisconsin

(Manuscript received 19 October 2009, in final form 11 May 2010)

ABSTRACT

The Moderate Resolution Imaging Spectroradiometer (MODIS) observations provide an unprecedented opportunity for studying cloud macrophysical (cloud-top pressure, temperature, height, and phase), microphysical (effective particle size), and optical (optical thickness) properties. Given the length of time these MODIS products have been available, it is found that the cloud products can provide a wealth of information about equatorial wave systems. In this study, more than six years of the MODIS cloud-top properties inferred from the *Aqua* MODIS observations are used to investigate equatorial waves. It is shown that the high-resolution daily gridded cloud-top temperature product can be used to quantitatively study convective clouds. Various modes of convectively coupled equatorial waves including Kelvin, $n = 1$ equatorial Rossby, mixed Rossby-gravity, $n = 0$ eastward inertial-gravity waves, and the Madden-Julian oscillation are identified on the basis of space-time spectral analysis. The application of spectral analysis to cirrus cloud optical thickness, retrieved from MODIS cirrus reflectance, confirms the convective signals at high altitudes. A cluster of Kelvin pulses is found to propagate eastward around the globe at a phase speed approximately 15 m s^{-1} . The Madden-Julian oscillation propagates at a slower speed and is most prominent over the Indian-Pacific Oceans region. The consistency between the present results with those of previous studies demonstrates that the MODIS cloud-top property products are valuable for studying phenomena associated with atmospheric dynamics.

1. Introduction

The Moderate Resolution Imaging Spectroradiometer (MODIS) sensors (King et al. 1992, 2003; Platnick et al. 2003) on board the National Aeronautics and Space Administration (NASA) Earth Observing System (EOS) *Terra* and *Aqua* platforms began to collect data in February 2000 and July 2002, respectively. The MODIS instrument has 36 spectral bands with nadir spatial resolutions of 250 m (2 bands), 500 m (5 bands), and 1000 m (29 bands). MODIS observes the entire earth within approximately two days at a scan rate of 20.3 rpm in the cross-track direction. Several algorithms have been developed

to infer cloud properties from MODIS observations (King et al. 1992; Platnick et al. 2003; Minnis et al. 1995, 1998). The recently released MODIS collection 5 (King et al. 2006) level 3 data provide gridded cloud properties on a daily, 8-day, and monthly basis at a global 1° longitude by 1° latitude resolution. The intent of the present study is to illustrate that the MODIS cloud-top retrieval products can be used to detect various equatorial wave signals.

Tropical convection (TC) systems play an important role in regulating the global hydrological cycle and energy budget. These TC systems are often organized in terms of equatorial waves (Takayabu 1994; Wheeler and Kiladis 1999, hereinafter WK99). Equatorial wave theory begins with separation of the primitive dynamic equations into horizontal shallow-water equations and the vertical propagation equation (Matsuno 1966). On an equatorial beta plane, different solutions to the linearized

Corresponding author address: Prof. Ping Yang, Department of Atmospheric Sciences, Texas A&M University, College Station, TX 77843.
E-mail: pyang@tamu.edu

shallow-water equations, for a resting basic state, correspond to the dispersion relations for a variety of equatorial waves. Satellite observations provide an unprecedented opportunity to study equatorial waves from a global perspective. Chang (1970) identified westward-moving equatorial wave disturbances over tropical oceans from satellite images. Other observational studies reported both westward- and eastward-propagating disturbances (Yanai and Murakami 1970; Reed and Recker 1971; Wallace and Chang 1972). WK99 conducted space–time spectral analysis on nearly 18 years of outgoing longwave radiation (OLR) data observed by the National Oceanic and Atmospheric Administration (NOAA) polar-orbiting satellites and isolated various equatorial wave modes, including the Madden–Julian oscillation (MJO), Kelvin, $n = 1$ equatorial Rossby (ER), mixed Rossby–gravity (MRG), and inertial-gravity (IG) waves. It should be emphasized that the MJO mode is not in agreement with any dispersion relation. Cho et al. (2004) applied spectral analysis to the Tropical Rainfall Measuring Mission satellite (TRMM) measured precipitation data and reported similar results. The focus of this note is on the analysis of TC systems from cloud-top properties rather than from OLR, which WK99 used as a proxy for clouds. Under clear or partially cloudy conditions, underlying surfaces may contaminate the cloud signal in OLR. From a remote sensing perspective when clouds are present, the magnitude of OLR is closely related to cloud-top temperature.

By using cloud products from a polar-orbiting imager such as MODIS to investigate various tropical waves, this work can be extended easily to cloud products based on heritage sensors such as the Advanced Very High Resolution Radiometer (AVHRR; Heidinger and Pavolonis 2009) and the High Resolution Infrared Radiation Sounder (HIRS; Wylie et al. 2005). Cloud products from these two sensors would extend the cloud product series back in time to about 1980.

2. Data and methodology

The MODIS *Aqua* daily cloud-top temperature (CTT) gridded product is analyzed from mid-July 2002 to early January 2009 between 15°N and 15°S. The CTT is retrieved both day and night and combined to get a daily average. Low values of CTT usually denote high clouds, which are prevalent over the tropics (Liou 1986; Rossow and Schiffer 1999; Wylie et al. 2005; Dessler and Yang 2003), and the fraction of deep convective clouds is about 15% of the total tropical high clouds (Hong et al. 2007). Cloud-top pressure (CTP) is inferred by the CO₂ slicing technique for clouds at pressures below about 700 hPa (Menzel et al. 2008; Wylie and Menzel 1999), and the CTT is determined subsequently through comparison with

gridded profiles from the National Centers for Environmental Prediction (NCEP) Global Data Assimilation System (GDAS) meteorological product (Derber et al. 1991). For low-level clouds, the infrared window 11- μm channel temperature is used to infer the CTT (Platnick et al. 2003). From the MODIS data, the CTT is not provided under clear-sky conditions or under conditions when a cloud is below a detectable limit (visible optical thickness of approximately 0.3). However, the spectral analysis requires data continuity with no gaps. One solution is to average over a large area, but spatial resolution would be reduced and averaging cannot eliminate all missing data. In this study, a neighbor filling method is used to estimate the missing data. Measurements within 1° latitude–longitude in each direction from the missing data points are examined and the available data averaged to fill the gaps. This process is repeated until all missing points have been filled. As missing data account for only about 2% of the selected spatial range and period, this filling procedure is not expected to introduce significant biases in the subsequent studies. We note that the OLR data used in WK99 were also interpolated to remove missing values (Liebmann and Smith 1996).

In addition, the MODIS *Aqua* gridded daily cirrus cloud optical thickness is investigated from September 2002 to September 2008. The cirrus clouds are generally located at the top of cloud layers at altitudes above 10 km. The dissipation of tropical deep convective cloud constitutes an important source for thin cirrus (Jensen et al. 1996). The cirrus optical thickness used in this study is inferred from operational MODIS cirrus reflectance based on MODIS band 26 at 1.38 μm (Gao et al. 2004; Meyer et al. 2007). This band is located near a strong water vapor absorption line; the signal tends to attenuate well above the surface in the tropics so that there is no contribution from low-level water clouds or aerosols. Thus the cirrus optical thickness inferred from this band is useful for spectral analysis of the high clouds.

The WK99 spectral analysis methodology is followed herein with a brief summary of the procedure. The data are divided into successive 96-day segments with 50 overlapping days. Equatorial waves are either symmetric or antisymmetric about the equator. Hence, for each segment, symmetric and antisymmetric components are separately computed with respect to the equator. Complex Fourier transform is performed in longitude and in time to obtain the wavenumber–frequency spectra of both the components, and the power is averaged over all segments. A background spectrum is computed by averaging the mean symmetric and antisymmetric components and then by smoothing many times. The spectral peaks are isolated by dividing each raw spectrum with the smoothed background spectrum.

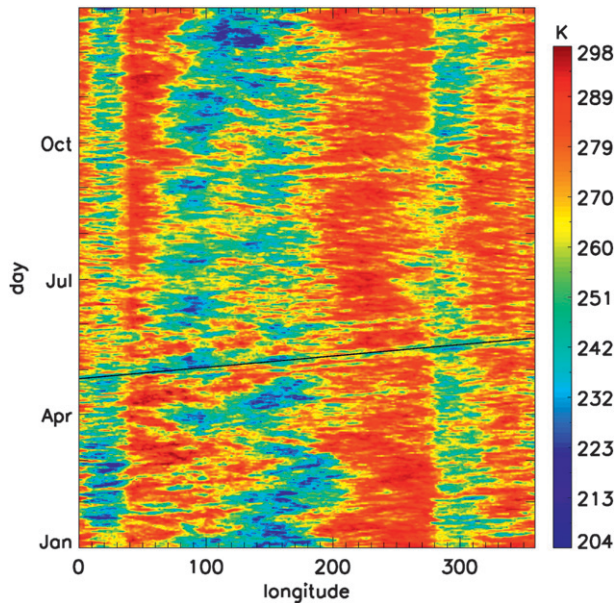


FIG. 1. Hovmöller diagram of raw CTT averaged between 15°N and 15°S of year 2005 from MODIS *Aqua* data. The thick line corresponds to phase speed 15 m s⁻¹.

3. Results

Figure 1 shows the Hovmöller diagram for the 2005 raw daily CTT averaged between 15°N and 15°S. Cold anomalies are observed in three distinct regions: central Africa (10°–40°E); the Indian Ocean and the warm pool western Pacific Ocean through central Pacific (80°–200°E); and South America (280°–320°E). High clouds are dominant over these regions (Hong et al. 2007). Cold anomalies over the Indian–Pacific region are stronger during the boreal winter than during the boreal summer. A cluster of convectively coupled Kelvin pulses propagates eastward around the tropics at a speed approximately 15 m s⁻¹, as illustrated by the thick line in Fig. 1. Westward-moving wave features are also evident, particularly in the Indian–Pacific region. For instance, a cold anomaly originates around 180°E in early January and propagates westward to 140°E. Several oscillating eastward–westward-propagating disturbances, indicating a mixture of different types of waves, are observed in this region from January to May.

Further insight is gained through the use of empirical orthogonal function (EOF) analysis, as shown in Fig. 2, which decomposes the space–time field into a space component and a time component. Since the extended EOF (EEOF) analysis incorporates time-lagged information, it is useful for studying wave generation and propagation (Weare and Nasstrom 1982; Hannachi et al. 2007; Roundy and Schreck 2009). A longitude–lag-day cross section of EEOF 5 of the CTT averaged between 5°N and 5°S

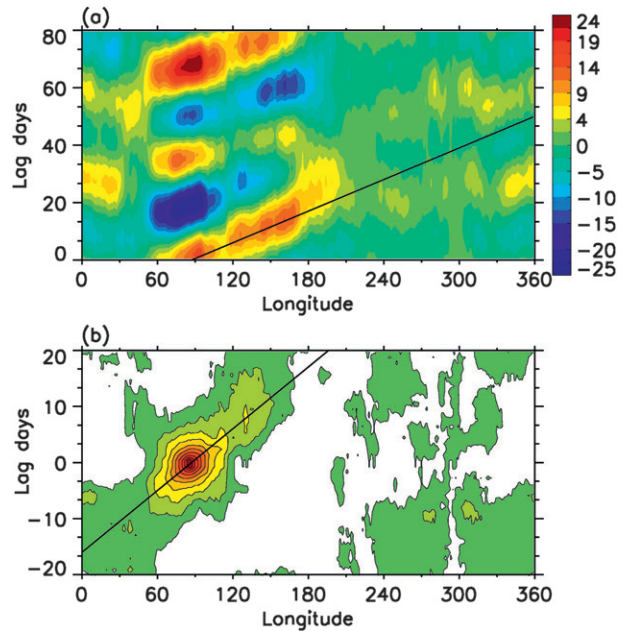


FIG. 2. (a) Longitude–lag-day cross section of EEOF 5 of CTT averaged between 5°N and 5°S. Units are arbitrary. (b) Lag correlation of the CTT anomaly averaged between 5°N and 5°S with respect to itself at 85°E. Shading starts at 0 and increases an interval of 0.1. The thick line corresponds to phase speed 7 m s⁻¹ in each figure.

is presented in Fig. 2a. Except EEOF 1, other leading EEOFs have similar patterns, but we chose EEOF 5 because it has the most pronounced trend. Seasonal cycles are first calculated by averaging over the years. Subsequently, anomalies are obtained by subtracting the seasonal cycle, and the EEOF is applied. A clear eastward-moving disturbance originates in the Indian Ocean, decays at the date line with an average phase speed of approximately 7 m s⁻¹, and indicates an MJO signal (Knutson and Weickmann 1987; Madden and Julian 1994). There is also an implication that the MJO breaks into two weak waves that continue to propagate eastward after passing the date line. Lin et al. (2006) used the time lag correlation to track MJO propagation and compared the observations with climate model simulations. Figure 2b shows the lag correlation of CTT anomaly averaged between 5°N and 5°S with respect to itself at 85°E. The observation indicates a distinct eastward-propagating MJO signal.

Figure 3a shows the autocorrelation for CTT averaged over a western Pacific warm pool region (15°N–15°S, 155°–165°E) as a function of time lag. Autocorrelation for 1200 lag days (approximately half of the data time series) is computed and the values for the first 500 lag days are plotted. A 1–2–1 filter is smoothed 20 times to remove noise, and the value at 0 lag is fixed at 1. In the first few

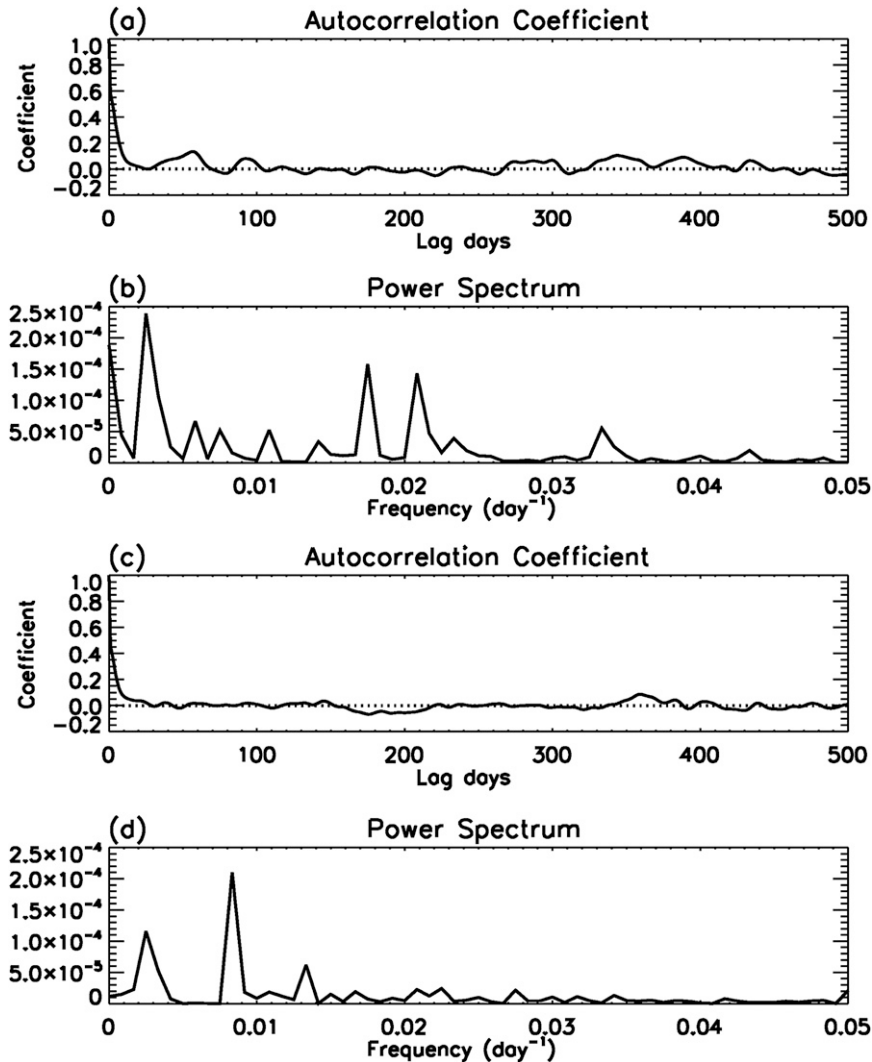


FIG. 3. (a) Autocorrelation of CTT averaged over the region 15°N–15°S, 155°–165°E. Here 1–2–1 smoothing is applied 20 times. The first value is not smoothed. (b) Power spectrum of autocorrelation in (a). Units are arbitrary. (c) As in (a), but averaged over 15°N–15°S, 240°–250°E. (d) Power spectrum of (c).

lag days, the autocorrelation decreases quickly to 0 because of the weakening of the self-memory effect. A further increase in the lag days increases the autocorrelation, exhibiting an oscillating pattern. This can be explained by the passage of various equatorial waves that cause the fluctuation of cloudiness, inducing the oscillation. The power spectrum of the autocorrelation series reveals many distinct peaks (see Fig. 3b). The most prominent peak corresponds to a period around 360 days and is associated with the annual cycle. The second and third peaks are both located in the 40–80-day period range, consistent with the period of the MJO. The equatorial wave activity is weaker in the eastern Pacific (15°N–15°S, 240°–250°E; Fig. 3c) than in the western Pacific

region. The oscillation period is longer and the oscillation magnitudes are smaller than their counterparts in Fig. 3a. The first peak in the power spectrum in Fig. 3d suggests the annual variation. The most distinct peak corresponds to a period of 125 days and is likely due to aliases. The spectral peak corresponding to the MJO is not as prominent as in Fig. 3b, indicating the weakening of the MJO signal in the eastern Pacific over the time period of the MODIS dataset.

Figure 4 shows the space–time power spectrum of the symmetric and antisymmetric components. The contours are the logarithm of the power summed over 15°N to 15°S. Since each data length for spectral analysis is 96 days, frequencies less than 1/96 cycles per day (cpd) are not

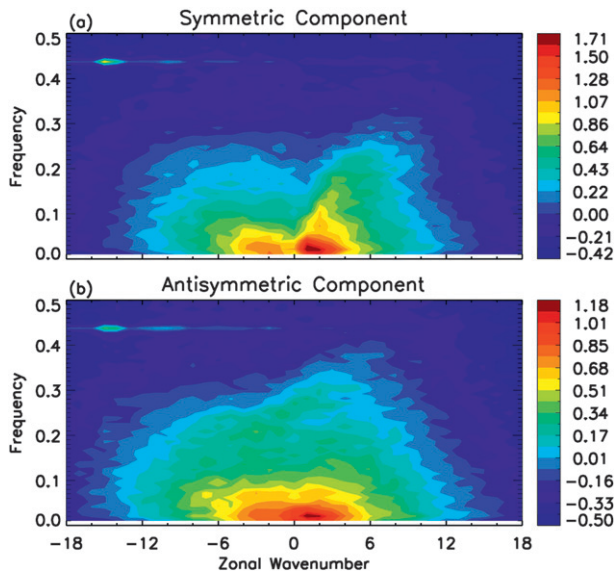


FIG. 4. Zonal wavenumber–frequency power spectra of the (a) symmetric and (b) antisymmetric components of MODIS *Aqua* CTT. For each component, the power is summed over 15°N–15°S, and the base-10 logarithm is taken.

plotted. An erroneous peak is detected around negative wavenumber 14, a period of 2.3 days in both the components. This may be associated with the number of swaths that MODIS *Aqua* observes each day, similar to the erroneous peaks pointed out in WK99. Successive peaks along the belt of about a 2.3-day period are also spurious and possibly related to the satellite orbit. In the computation of the background spectrum and isolation of spectral peaks discussed later, the negative wavenumber 14 peak will be removed but the remaining 2.3-day belt will be kept. Some prominent features can be identified, especially for the symmetric component. One distinct feature is the dominance of a spectral peak in eastward wavenumber 1–4 at low frequencies over the westward component that is related to the strong eastward-propagating MJO (Zhang 2005; Lin et al. 2006). Other strong spectral peaks, namely the “ridges” of individual curves, can be identified visually—particularly Kelvin, $n = 1$ ER, MRG, and $n = 0$ eastward IG (EIG) wave dispersion curves—and are more clearly shown in Fig. 5.

Various equatorial wave modes are obtained by dividing the mean symmetric and antisymmetric components to the background spectrum, respectively (Fig. 5). The background spectrum is obtained by averaging the mean symmetric and antisymmetric parts and both wavenumber and frequency are smoothed numerous times with a 1–2–1 filter. The number of smoothing times in wavenumber is 5 at frequencies less than 0.1 and 40 at frequencies larger than 0.4 increasing in two different steps, whereas it is applied 10 times throughout in the

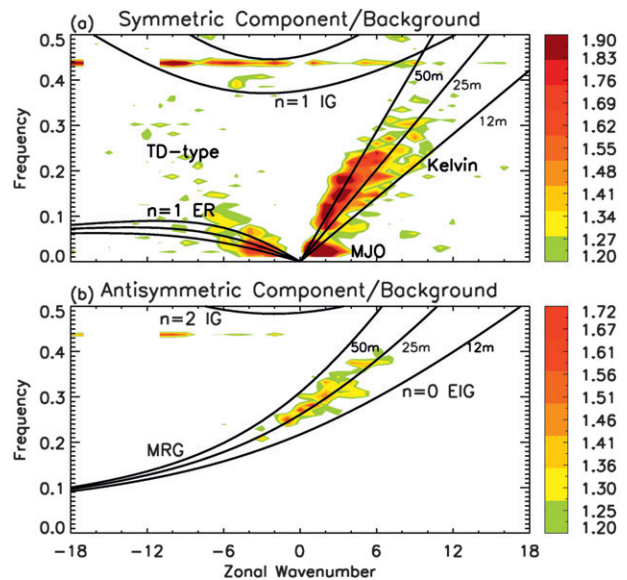


FIG. 5. (a) The mean symmetric and (b) antisymmetric component power spectrum divided by the background spectrum. The background power is smoothed by a 1–2–1 filter many times. An erroneous peak near negative wavenumber 14 is not plotted.

frequency spectrum. Superimposed curves correspond to dispersion relations of various equatorial waves with motionless basic state and three equivalent thicknesses: 12, 25, and 50 m. In WK99, ratios larger than 1.1 are considered statistically significant. As the span of data in this study is shorter, 1.2 is adopted as the significance threshold. Consistent with WK99, 25 m is the optimal equivalent thickness. The phase speed of this equivalent depth is slower than that of the free waves in the equatorial stratosphere, and WK99 explained this in terms of the interaction between convection and dynamics. The exception is the equatorial Kelvin wave, where the spectral peaks are seen along the equivalent depth of 50 m for wavenumber 1–4. However, with increasing wavenumber, the equivalent depth of 25 m appears to be a better match. This phenomenon is also observed in WK99. Kelvin, $n = 1$ ER, MRG, and $n = 0$ EIG waves clearly stand out above the background. The MJO signal of eastward wavenumber 1–4, with periods of 30–100 days, is well separated from the Kelvin wave in the symmetric component.

Also of interest is a wave associated with tropical depressions (TD) that may be observed in the westward wavenumber of the symmetric component. The TD-type waves, also known as easterly waves, are important in the genesis and formation of tropical cyclones (Dunn 1940; Riehl 1948). Weak $n = 1$ IG waves are present in the symmetric component. However, it should be emphasized that the signals along the 2.3-day belt may be

contaminated by the satellite orbit instead of indicating the IG signal. This will be explored further in future research with a longer time series of cloud products.

Overshooting tropical convection systems can penetrate to very high altitudes, even above the tropopause, generating cirrus clouds through convective blowoff and indirectly altering the upper-level temperature and moisture fields. This dynamic process links the equatorial waves and high cirrus clouds. Figure 6 shows the power spectrum for various equatorial waves after applying spectral analysis to cirrus optical thickness. Since missing data occupy a much larger portion than in the CTT (about 27.8%), some noise may be expected to be introduced after filling the gaps. Accordingly, the significance threshold is reduced to 1.1. Figure 6 indicates that equatorial wave modes clearly stand out from the background, confirming that convective signals in equatorial regions are pronounced in high cirrus. However, all wave signals, except MJO in the symmetric component, are weaker with respect to the background compared to those in Fig. 5. The MJO signal is also observed in the antisymmetric part. Eguchi and Shiotani (2004) examined the tropical upper-tropospheric water vapor and cirrus clouds associated with MJO and reported that cirrus clouds are closely related to high humidity and cold anomalies because of the convective center. Fujiwara et al. (2009) investigated the cirrus variations over the tropical western Pacific in the tropical tropopause layer using lidar radiosonde data and revealed that equatorial waves play a major role in generating and dissipating cirrus clouds. Our results are consistent with these studies. The relatively weak signal in the power spectrum suggests that a portion of cirrus may be formed in situ, but this may be due in part to the large portion of missing data.

4. Summary and discussion

To illustrate the wealth of information that the MODIS cloud retrieval products provide about atmospheric dynamical phenomena, more than 6 years of MODIS cloud-top properties from the *Aqua* platform, specifically cloud-top temperature and cirrus optical thickness, are used to study equatorial wave properties. A space-time spectral analysis is conducted based on the level 3 daily product. Various equatorial wave modes are identified, such as Kelvin wave, $n = 1$ equatorial Rossby and MRG waves, $n = 0$ EIG and $n = 1$ IG waves, and the MJO waves. Also found are waves associated with tropical depressions. A cluster of convectively coupled Kelvin wave pulses is found to move at a phase speed of approximately 15 m s^{-1} around the globe, whereas the MJO is slower (about 7 m s^{-1}) and more confined to the Indian–Pacific region. Consistent with previous findings,

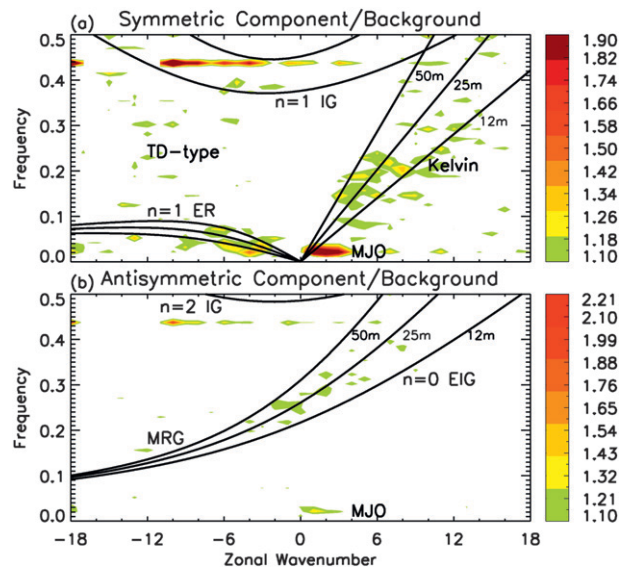


FIG. 6. As in Fig. 5, except using cirrus optical depth.

an equivalent depth of 25 m is optimal for these convectively coupled equatorial waves. Perhaps because of spatial gaps in MODIS coverage in the tropics for a single day, some spurious peaks are present, raising the issue that interpretation must be carefully made. Further studies using other MODIS gridded products will be necessary to answer the question. Roundy and Frank (2004) analyzed the daily total column precipitable water (PW) datasets from the NASA Water Vapor Project and demonstrated that a zonal phase shift between the OLR and PW anomalies is related to equatorial waves. The answer to whether the equatorial wave signals can be detected in the MODIS water vapor product may contribute to a better understanding of the interaction of different phenomena inherent in the development and propagation of various equatorial waves. More continuous MODIS observations are needed to study interannual to decadal oscillations of the atmosphere, such as the quasi-biennial oscillation (QBO) (Baldwin et al. 2001). It would also be useful to extend the MODIS analysis to the longer-term decadal cloud products available from AVHRR (Heidinger and Pavolonis 2009). Our effort demonstrates that MODIS cloud products are valuable in the study of the tropical dynamics of the atmosphere. The use of cloud products rather than OLR as a proxy for cloud cover suggests that more detailed analyses can be explored to take advantage of vertical cloud structures. The study on the relationship between cirrus clouds and equatorial waves is important to understand upper-level cloud behaviors and provides insights to better represent cirrus clouds in climate models. Furthermore, the cloud and water vapor products from MODIS can be

used to improve the understanding of the phenomena associated with atmospheric dynamics, with no regional limits, because of the high spatial resolution and global coverage provided by various polar-orbiting satellite imagers.

Acknowledgments. This research is supported by a research grant from NASA (NNX08AF68G) from NASA Radiation Sciences Program managed by Dr. Hal Maring and the MODIS Program managed by Dr. Paula Bontempi. We thank Dr. Matthew Wheeler for providing the codes. The cirrus optical thickness data are generously provided by Dr. Kerry Meyer. We also thank Dr. Matthew Wheeler, Dr. Jianhua Huang, and Bingqi Yi for helpful discussions.

REFERENCES

- Baldwin, M. P., and Coauthors, 2001: The quasi-biennial oscillation. *Rev. Geophys.*, **39**, 179–229.
- Chang, C. P., 1970: Westward propagating cloud patterns in the tropical Pacific as seen from time composite satellite photographs. *J. Atmos. Sci.*, **27**, 133–138.
- Cho, H. K., K. P. Bowman, and G. R. North, 2004: Equatorial waves including the Madden–Julian oscillation in TRMM rainfall and OLR data. *J. Climate*, **17**, 4387–4406.
- Derber, J. C., D. F. Parrish, and S. J. Lord, 1991: The new global operational analysis system at the National Meteorological Center. *Wea. Forecasting*, **6**, 538–547.
- Dessler, A. E., and P. Yang, 2003: The distribution of tropical thin cirrus clouds inferred from Terra MODIS data. *J. Climate*, **16**, 1241–1247.
- Dunn, G. E., 1940: Cyclogenesis in the tropical Atlantic. *Bull. Amer. Meteor. Soc.*, **21**, 215–229.
- Eguchi, N., and M. Shiotani, 2004: Intraseasonal variations of water vapor and cirrus clouds in the tropical upper troposphere. *J. Geophys. Res.*, **109**, D12106, doi:10.1029/2003JD004314.
- Fujiwara, M., and Coauthors, 2009: Cirrus observations in the tropical tropopause layer over the western Pacific. *J. Geophys. Res.*, **114**, D09304, doi:10.1029/2008JD011040.
- Gao, B.-C., K. Meyer, and P. Yang, 2004: A new concept on remote sensing of cirrus optical depth and effective ice particle size using strong water vapor absorption channels near 1.38 and 1.88 μm . *IEEE Trans. Geosci. Remote Sens.*, **42**, 1891–1899.
- Hannachi, A., I. T. Jolliffe, and D. B. Stephenson, 2007: Empirical orthogonal functions and related techniques in atmospheric science: A review. *Int. J. Climatol.*, **27**, 1119–1152.
- Heidinger, A. K., and M. J. Pavolonis, 2009: Gazing at cirrus clouds for 25 years through a split window. Part I: Methodology. *J. Appl. Meteor. Climatol.*, **48**, 1100–1116.
- Hong, G., P. Yang, B.-C. Gao, B. A. Baum, Y. X. Hu, M. D. King, and S. Platnick, 2007: High cloud properties from three years of MODIS Terra and Aqua collection-4 data over the tropics. *J. Appl. Meteor. Climatol.*, **46**, 1840–1856.
- Jensen, E. J., O. B. Toon, H. B. Selkirk, J. D. Spinhirne, and M. R. Schoeberl, 1996: On the formation and persistence of subsvisible cirrus clouds near the tropical tropopause. *J. Geophys. Res.*, **101** (D16), 21 361–21 375.
- King, M. D., Y. J. Kaufman, W. P. Menzel, and D. Tanre, 1992: Remote sensing of cloud, aerosol, and water vapor properties from the Moderate Resolution Imaging Spectrometer (MODIS). *IEEE Trans. Geosci. Remote Sens.*, **30**, 2–27.
- , and Coauthors, 2003: Cloud and aerosol properties, precipitable water, and profiles of temperature and water vapor from MODIS. *IEEE Trans. Geosci. Remote Sens.*, **41**, 442–458.
- , S. Platnick, P. A. Hubanks, G. T. Arnold, E. G. Moody, G. Wind, and B. Wind, cited 2006: Collection 005 change summary for the MODIS cloud optical property (06_OD) algorithm. [Available online at http://modis-atmos.gsfc.nasa.gov/C005_Changes/C005_CloudOpticalProperties_ver311.pdf.]
- Knutson, T. R., and K. M. Weickmann, 1987: 30–60 day atmospheric oscillation: composite life cycles of convection and circulation anomalies. *Mon. Wea. Rev.*, **115**, 1407–1436.
- Liebmann, B., and C. A. Smith, 1996: Description of a complete (interpolated) outgoing longwave radiation dataset. *Bull. Amer. Meteor. Soc.*, **77**, 1275–1277.
- Lin, J.-L., and Coauthors, 2006: Tropical intraseasonal variability in 14 IPCC AR4 climate models. Part I: Convective signals. *J. Climate*, **19**, 2665–2690.
- Liou, K.-N., 1986: Influence of cirrus clouds on weather and climate processes: A global perspective. *Mon. Wea. Rev.*, **114**, 1167–1199.
- Madden, R. A., and P. R. Julian, 1994: Observation of the 40–50-day tropical oscillation—A review. *Mon. Wea. Rev.*, **122**, 814–837.
- Matsuno, T., 1966: Quasi-geostrophic motions in the equatorial area. *J. Meteor. Soc. Japan*, **44**, 25–43.
- Menzel, W. P., and Coauthors, 2008: MODIS global cloud-top pressure and amount estimation: Algorithm description and results. *J. Appl. Meteor. Climatol.*, **47**, 1175–1198.
- Meyer, K., P. Yang, and B.-C. Gao, 2007: Ice cloud optical depth from MODIS cirrus reflectance. *IEEE Trans. Geosci. Remote Sens.*, **4**, 471–474.
- Minnis, P., and Coauthors, 1995: Cloud optical property retrieval (subsystem 4.3). *Cloud Analyses and Radiance Inversions (Subsystem 4)*, CERES Science Team, Eds., Vol. III, *Clouds and the Earth's Radiant Energy System (CERES) Algorithm Theoretical Basis Document*, NASA RP 1376, 135–176.
- , D. P. Garber, D. F. Young, R. F. Arduini, and Y. Takano, 1998: Parameterizations of reflectance and effective emittance for satellite remote sensing of cloud properties. *J. Atmos. Sci.*, **55**, 3313–3339.
- Platnick, S., M. D. King, S. A. Ackerman, W. P. Menzel, B. A. Baum, J. C. Riedi, and R. A. Frey, 2003: The MODIS cloud products: Algorithms and examples from Terra. *IEEE Trans. Geosci. Remote Sens.*, **41**, 459–473.
- Reed, R. J., and E. E. Recker, 1971: Structure and properties of synoptic-scale wave disturbances in the equatorial western Pacific. *J. Atmos. Sci.*, **28**, 1117–1133.
- Riehl, H., 1948: On the formation of typhoons. *J. Meteor.*, **5**, 247–265.
- Rossow, W. B., and R. A. Schiffer, 1999: Advances in understanding clouds from ISCCP. *Bull. Amer. Meteor. Soc.*, **80**, 2261–2287.
- Roundy, P. E., and W. M. Frank, 2004: A climatology of waves in the equatorial region. *J. Atmos. Sci.*, **61**, 2105–2132.
- , and C. J. Schreck III, 2009: A combined wave-number-frequency and time-extended EOF approach for tracking the progress of modes of large-scale organized tropical convection. *Quart. J. Roy. Meteor. Soc.*, **135**, 161–173.
- Takayabu, Y. N., 1994: Large-scale cloud disturbances associated with equatorial waves. Part I: Spectral features of the cloud disturbances. *J. Meteor. Soc. Japan*, **72**, 433–448.

- Wallace, J. M., and L. A. Chang, 1972: On the application of satellite data on the cloud brightness to the study of tropical wave disturbances. *J. Atmos. Sci.*, **29**, 1400–1403.
- Weare, B. C., and J. S. Nasstrom, 1982: Examples of extended empirical orthogonal function analysis. *Mon. Wea. Rev.*, **110**, 481–485.
- Wheeler, M. C., and G. N. Kiladis, 1999: Convectively coupled equatorial waves: Analysis of cloud and temperature in the wavenumber-frequency domain. *J. Atmos. Sci.*, **56**, 374–399.
- Wylie, D. P., and W. P. Menzel, 1999: Eight years of high cloud statistics using HIRS. *J. Climate*, **12**, 170–184.
- , D. L. Jackson, W. P. Menzel, and J. J. Bates, 2005: Trends in global cloud cover in two decades of HIRS observations. *J. Climate*, **18**, 3021–3031.
- Yanai, M., and M. Murakami, 1970: A further study of tropical wave disturbances by the use of spectrum analysis. *J. Meteor. Soc. Japan*, **48**, 185–197.
- Zhang, C., 2005: Madden–Julian oscillation. *Rev. Geophys.*, **43**, RG2003, doi:10.1029/2004RG000158.